Journal of the Indian Society of Remote Sensing (April 2018) 46(4):591–596
https://doi.org/10.1007/s12524-017-0713-7

RESEARCH ARTICLE

Is There a Physical Linkage Between Surface Emissive and Reflective Variables Over Non-Vegetated Surfaces?

Jie Cheng[1,2] · Shunlin Liang[1,2] · Aixiu Nie[3] · Qiang Liu[3]

Received: 7 November 2016 / Accepted: 3 October 2017 / Published online: 2 December 2017

Abstract

For a satellite sensor with only one or two thermal infrared channels, it is difficult to retrieve the surface emissivity from the received emissive signal. Empirical linear relationship between surface emissivity and red reflectance are already established for deriving emissivity, but the inner physical mechanism remains unclear. The optical constants of various minerals that cover the spectral range from 0.44 to 13.5 μm in conjunction with modern radiative transfer models were used to produce corresponding surface reflectance and emissivity spectra. Compared to the commonly used empirical linear relationship, a more accurate multiple linear relationship between Landsat TM5 emissivity and optical reflectances was derived using the simulated data, which indicated the necessity of replacing the empirical relationship with the new one for improving surface emissivity estimate in the single channel algorithm. The significant multiple linear relationship between broadband emissivity (BBE, 8–13.5 μm) and MODIS spectral albedos was also derived using the same data. This paper demonstrates that there is a physical linkage between surface emissive and reflective variables, and provides a theoretical perspective on estimating surface emissivity for sensors with only one or two thermal infrared channels.

Keywords Optical constant · Kirchhoff's law · NDVI · Reflectance · Emissivity · Radiative transfer theory

Introduction

According to Kirchhoff's law, a complementary relationship exists between surface emissivity and reflectance, which allows the emissivity to be calculated from the reflectance that is often more convenient to measure in the laboratory (Hapke 2012). For example, one can calculate the directional emissivity spectra of various natural and manmade materials from the laboratory-measured hemispherical-directional reflectance in the ASTER spectral library (Baldridge et al. 2009) by virtue of Kirchhoff's law. Regarding satellite remote sensing, the earth observation thermal infrared sensor primarily measures the emissive signal of the surface and atmosphere instead of the reflective signal. It is impossible to derive the surface reflectance for the received emissive signal. Thus, we cannot derive the surface emissivity using Kirchhoff's law.

We must resort to alternative methods that can derive surface emissivity directly from sensor-measured emissive signals. One alternative is the so-called temperature and emissivity separation (TES) algorithm. Temperature and emissivity separation from radiometric measurements is an ill-posed problem, which involves solving N + 1 variables

Jie Cheng and Shunlin Liang jointly sponsored by Beijing Normal University and Institute of Remote Sensing and Digital Earth of Chinese Academy of Sciences.

✉ Jie Cheng
brucechan2003@126.com

Shunlin Liang
sliang@bnu.edu.cn

Aixiu Nie
nieaixiu@126.com

Qiang Liu
toliuqiang@bnu.edu.cn

[1] State Key Laboratory of Remote Sensing Science, Beijing Normal University and Institute of Remote Sensing and Digital Earth of Chinese Academy of Sciences, Beijing 100875, China

[2] Institute of Remote Sensing Science and Engineering, Faculty of Geographical Science, Beijing Normal University, Beijing 100875, China

[3] College of Global Change and Earth System Science, Beijing Normal University, Beijing 100875, China

with N equations (Cheng et al. 2011; Gillespie et al. 1998; Li et al. 1999; Li et al. 2013a; Xue et al. 2005). A larger number of TES algorithms have been developed to derive surface emissivity from the measured emissive signal (Cheng and Ren 2012; Li et al. 2013b; Liang 2001). Typically, we design a specified TES algorithm for a sensor with three or more thermal infrared channels and derive the surface temperature and emissivity simultaneously, for example, the ASTER TES algorithm and MODIS day/night algorithm (Gillespie et al. 1998; Wan and Li 1997). However, it is difficult to derive the temperature and/or emissivity for a thermal infrared sensor with one or two channels. We must make use of the information measured by the synchronized optical remote sensing sensor. This is another alternative method. For example, the vegetation cover method (Valor and Caselles 1996) and NDVI-threshold method (Sobrino et al. 2008) are used to predetermine surface emissivity and then retrieve the surface temperature for Landsat TM/ETM+ in the single channel algorithm (Cristobal et al. 2009; Zhou et al. 2012). In the vegetation cover method or NDVI-threshold method, land surface is primarily divided into vegetated surface and non-vegetated surface. For the non-vegetated surface, the emissivity is assigned a constant value usually averaged from the soil emissivity spectra or fitted as a linear function of red reflectance using the spectra in the ASTER spectral library without allowing for the dramatic variation of non-vegetated surface emissivity. The linear relationship may not be entirely accurate, but it is definitely superior to the constant value. The emissivity of the partial vegetated surface is determined by introducing the components' (soil and vegetation) emissivity into a physical model that defines the effective emissivity of the surface in terms of an estimated vegetation fraction dynamically obtained from NDVI. Sobrino et al. (Sobrino et al. 2008) reviewed the development of the NDVI-threshold method and proposed the linear formulae for various thermal infrared sensors. The surface emissivity determined by the vegetation cover and NDVI-threshold methods have been successfully applied to the retrieval of surface temperatures from single-channel thermal infrared sensors such as Landsat TM/ETM+ with an desired accuracy of 1–2 K (Jimenez-Munoz et al. 2009; Qin and Karnieli 2001).

The study of Cheng and Liang (Cheng and Liang 2014) demonstrated that the accuracy of predicting BBE with seven MODIS spectral albedos was better than that using any single spectral albedo, because the information provided by single spectral albedo is limited. They established multiple linear relationships between BBE and seven MODIS spectral albedos for non-vegetated surfaces at a 1 km spatial resolution as well as between BBE and AVHRR visible and near-infrared channel reflectances (Cheng and Liang 2013, 2014). These relationships were adopted to produce operational global BBE products with spatiotemporal resolutions of eight days and1 km and 0.05° from MODIS and AVHRR optical data, from 1981 to 2015 (Liang et al. 2013). The eight-day, 1 km BBE derived from MODIS spectral albedos has a validation accuracy of 0.02 at pseudo-invariant sand dune sites (Dong et al. 2013). This global spatial–temporal complete BBE dataset facilitates the study of surface radiation energy balance at both global and regional scales.

Certainly, the incorporation of other channels in optical spectral range can improve the accuracy of surface emissivity estimation and further the accuracy of LST estimation. However, researchers are still prone to use red reflectance to calculate surface emissivity (Tardy et al. 2016). One of the reasons may be that the physical connection between surface emissive and reflective variables is unclear. Whether a physical connection exists between surface emissive and reflective variables remains unknown. The purpose of this study is to explore this relationship from the point of radiative transfer theory, which is the basis of quantitative remote sensing.

Method

The optical constants of various minerals that cover the spectral range from 0.44 to 13.5 μm in conjunction with modern radiative transfer models were used to produce surface reflectance and emissivity spectra. The relationship between surface emissive and reflective variables was investigated using the simulated data. Figure 1 shows the flowchart of our method. The optical constants of the various minerals and the effective radius of the particles are

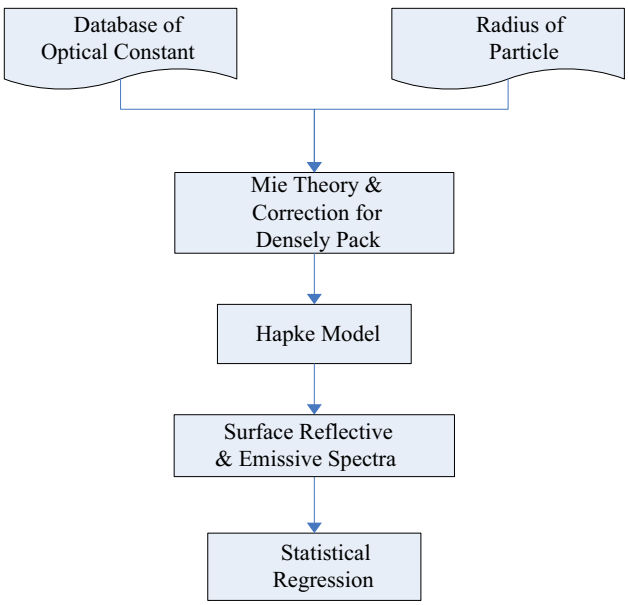

Fig. 1 The flowchart for investigating the physical linkage between surface reflectance and emissivity

input into the Mie Code to produce Mie parameters (the single-scatter albedo and asymmetry factors) for single particle (Mie 1908; Mishchenko et al. 2002); then, the dense-packing effects are considered using a static structure factor correction (Mishchenko and Macke 1997). The corrected Mie parameters are then input into modern radiative transfer model, the Hapke model (Hapke 2012), to produce the simulated nadir viewing surface reflectance and emissivity since the Hapke model has good performance in simulating directional reflectance and emissivity for semi-infinite media (Cheng et al. 2010; Pitman et al. 2005). The simulated surface reflectance and emissivity spectra are used to analyse the relationship between surface emissive and reflective variables.

The optical constant comes from the Jena—St. Petersburg database of Optical Constants (JPDOC, http://www.astro.spbu.ru/JPDOC/f-dbase.html). The database contains references to the papers, data files and links to Internet resources related to measurements and calculations of the optical constants in the wavelength interval from X-rays to the radio domain. The materials considered are amorphous and crystalline silicates of different types, various ices, oxides, sulfides, carbides, carbonaceous species from amorphous carbon to graphite and diamonds and some other materials of astrophysical and terrestrial atmospheric interest. The data on different minerals that could be downloaded from the website in the spectral range from 0.44 to 13.5 μm were adopted. In total, we obtained 42 samples, including silicates, oxides, sulfides, etc. The optical constants of the selected minerals are shown in Fig. 2.

Results and Discussion

The Mie code was used to simulate the Mie parameters for a single particle assuming that the effective radius of the particle was 50 μm for the purpose of saving computation time. Figure 3 shows the simulated Mie parameters. The spectral range of surface reflectance ranged from 0.44 to 2.18 μm, covering the spectral range of seven MODIS optical channels. The spectral range of surface emissivity was 8–13.5 μm. The single-scatter albedo and asymmetry factor both have large variations. The simulated Mie parameters were corrected for the dense packing of particles using the static structure factor correction (the filling factor was set as 0.2) and then input into the Hapke model. The formulae of Hapke reflective and emissive model are provided as below with the assumption that the particles emit and scatter isotropically (Hapke 2012).

$$r_{hd}(e) = (1-\gamma)/(1+2\gamma\mu) \quad (1)$$

$$\varepsilon_d(e) = \gamma\frac{1+2\mu}{1+2\gamma\mu} \quad (2)$$

where $r_{hd}(e)$ and $\varepsilon_d(e)$ and hemisphere-directional reflectance and directional emissivity; $\mu = cos(e)$ and e is viewing zenith angle; $\gamma = \sqrt{1-w}$ and w is the particle single scattering albedo. The simulated nadir viewing surface reflectance and emissivity spectra are shown in Fig. 4. The shape of the simulated surface reflectance spectra was similar to that of soil and rocks, but it had a large variation that ranges from approximately 0.15 to 0.7. Most of the simulated emissivity spectra had a high value except for several emissivity spectra in the spectral range of 11–13.5 μm. Note that the well-known "Reststrahlen Bands", a broad minimum of emissivity in silica minerals associated with interatomic stretching vibrations of Si and O bound in the crystal lattice (Gillespie 2014), did not appear in the simulated emissivity spectra. The Hapke model is capable of reproducing the shape of "Reststrahlen Bands"(Garcia-Santos

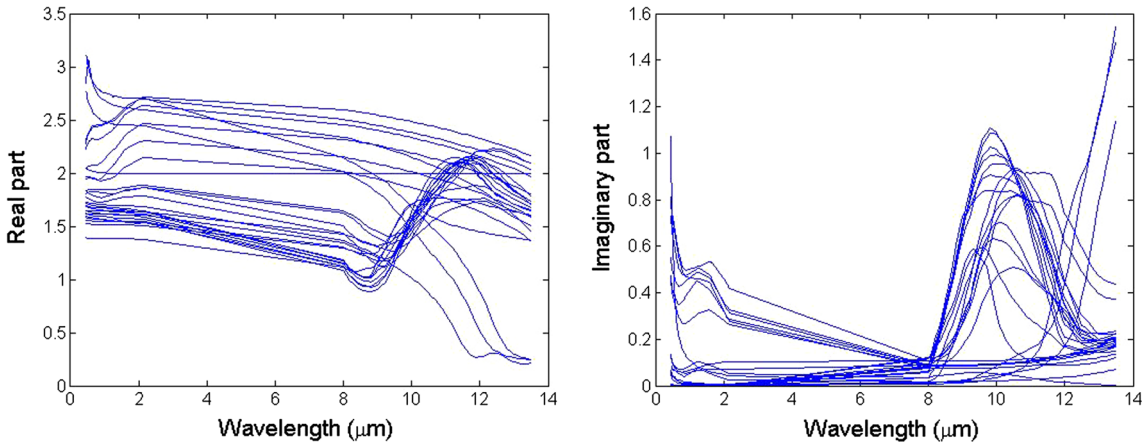

Fig. 2 The optical constants of selected minerals from JPDOC

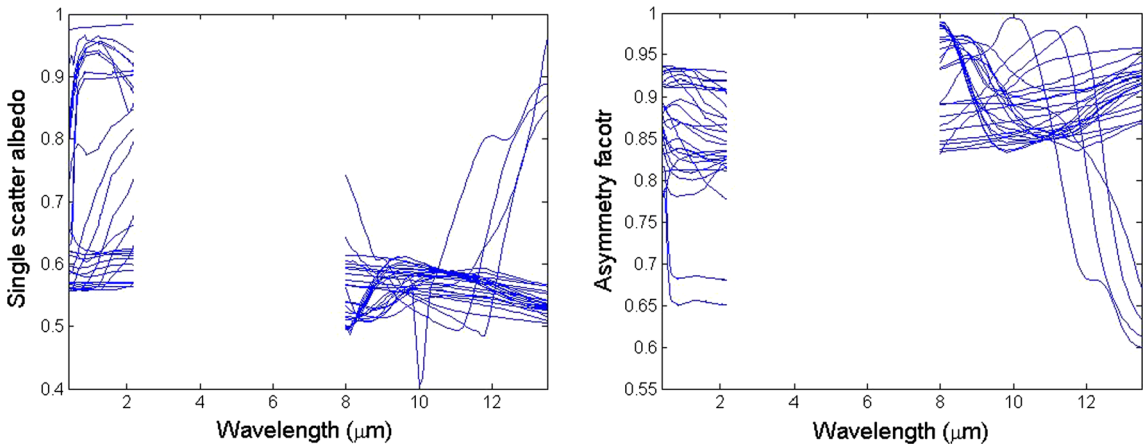

Fig. 3 The single-scattering albedo and asymmetry factor simulated by the Mie code

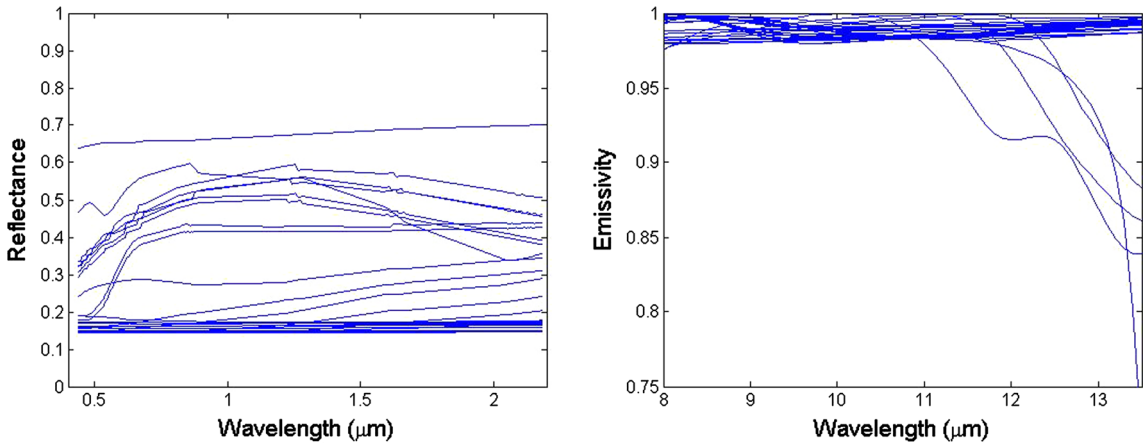

Fig. 4 The reflectance and emissivity spectra simulated by the Hapke Model

et al. 2016; Pitman et al. 2005). The "Restrahlen Bands" in the emissivity spectrum of silica (quartz) is determined by its optical constant. The optical constant of the collected samples in this study are different from the optical constant of silica (quartz) (Spitzer and Kleinman 1961). Thus, "Restrahlen Bands" is not presented in the simulated emissivity spectra.

The simulated surface reflectance spectra were convolved with the filter functions of seven optical channels of Landsat TM5 to generate the corresponding channel reflectances and emissivity. The linear relationship between emissivity and red reflectance was very weak, but a significant multiple linear relationship was found:

$$\varepsilon = 0.988 - 0.496R_1 + 1.186R_2 - 0.737R_3 \quad (3)$$

where ε is the emissivity of channel 6 and R_i is the Landsat reflectance for channel i. The formula and the coefficient for each variable are significantly below the confidence level of $P < 0.05$. The determination coefficient is 0.811. The bias and RMSE are 0.001 and 0.006, respectively. The fitting results are shown in Fig. 5. The simulated surface reflectance

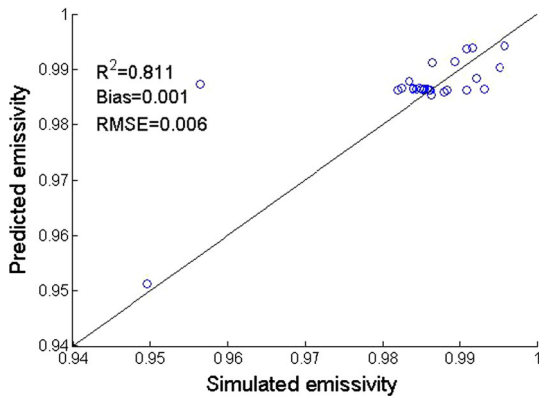

Fig. 5 The scatterplot of simulated emissivity versus the predicted emissivity using Eq. (3)

spectra were also convolved with the filter functions of MODIS seven optical channels to produce the corresponding spectral albedos assuming surface is lambertian.

In addition, the surface BBE was calculated from the simulated emissivity spectra assigned surface temperature

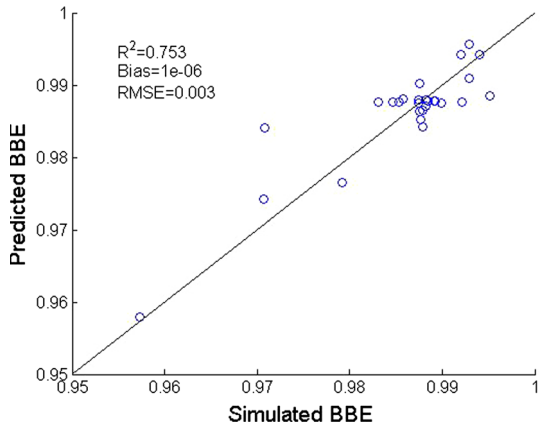

Fig. 6 The relationship between simulated broadband emissivity and the predicted broadband emissivity using Eq. (4)

as 300 K (Cheng et al. 2013). After obtaining the surface spectral albedos and BBE, a significant multiple linear function was derived:

$$\varepsilon_{bb} = 0.989 - 0.292\alpha_1 - 0.377\alpha_3 + 0.688\alpha_4 - 0.027\alpha_7 \quad (4)$$

where ε_{bb} is the BBE, and α_i is the MODIS spectral albedo for channel i. The determination coefficient is 0.753. The bias and RMSE are 1e-6 and 0.003, respectively. The fitting results are shown in Fig. 6. Clearly, a physical linkage exists between surface emissive and reflective variables.

To our knowledge, this is the first time the physical linkage between surface emissive and reflective variables has been clarified based on radiative transfer theory. Although many optical constants exist in the JPDOC, data covering the spectral range of 0.44–13.5 μm are very scarce. Thus, the number of samples used in this study is limited. If new data become available, we will incorporate them and re-examine the linkage. On the other hand, minerals are only one of the components of soil and rocks and cannot fully represent non-vegetated surfaces. Thus, the established formula may be unstable, and the fitting results may not always be acceptable. But formulating emissivity as a multiple linear function of channel reflectances is still better than the currently used constant assumption or a linear function of red reflectance over non-vegetated surfaces. Thus, we strongly suggested to replace the red reflectance by a multiple linear function of reflectances in optical region for estimating surface emissivity in the single channel algorithm.

Summary

For a sensor with only one or two thermal infrared channels, it is difficult to retrieve the surface emissivity from the received emissive signal. An empirical relationship between surface emissivity and red reflectance is established for predetermining surface emissivity to retrieve LST. This study attempted to explore their inner physical basis with the help of radiative transfer theory.

The optical constants of various minerals that cover the spectral range from 0.44 to 13.5 μm were downloaded from the JPDOC database. With these optical constant data, the Mie parameters (single-scatter albedo and asymmetry factor) were calculated with the Mie code and input into the Hapke model after correction for densely packed particles to produce surface reflectance and emissivity spectra. With these spectra, the channel reflectance and emissivity for Landsat TM5 were produced and used to analyse their relationship. The linear relationship between emissivity and red reflectance was very weak, but a more accurate function that expressed surface emissivity as a multiple linear function of reflectances was derived. The corresponding BBE and MODIS spectral albedos was also calculated and used to investigate their relationship, and similar results were obtained.

This paper demonstrates that there is a physical linkage between surface emissive and reflective variables, and provides a theoretical perspective on estimating emissivity for a sensor with only one or two thermal infrared channels.

Acknowledgements Optical constant optical data were obtained from http://www.astro.spbu.ru/JPDOC/f-dbase.html. This work was supported by the National Natural Science Foundation of China (No. 41771365 and No. 41371323) and the National Key Research and Development Program of China (No.2016YFA0600101).

References

Baldridge, A. M., Hook, S. J., Grove, C. I., & Rivera, G. (2009). The ASTER spectral library version 2.0. *Remote Sensing of Environment, 113,* 711–715.

Cheng, J., & Liang, S. (2013). Estimating global land surface broadband thermal-infrared emissivity from the advanced very high resolution radiometer optical data. *International Journal of Digital Earth, 6,* 34–49.

Cheng, J., & Liang, S. (2014). Estimating the broadband longwave emissivity of global bare soil from the MODIS shortwave albedo product. *Journal of Geophysical Research Atmosphere, 119,* 614–634.

Cheng, J., Liang, S., Liu, Q., & Li, X. (2011). Temperature and emissivity separation from ground-based MIR hyperspectral data. *IEEE Transactions on Geoscience and Remote Sensing, 49,* 1473–1484.

Cheng, J., Liang, S., Weng, F., Wang, J., & Li, X. (2010). Comparison of radiative transfer models for simulating snow surface thermal infrared emissivity. *IEEE Journal of Selected Topics in Earth Observations and Remote Sensing, 3,* 323–336.

Cheng, J., Liang, S., Yao, Y., & Zhang, X. (2013). Estimating the optimal broadband emissivity spectral range for calculating surface longwave net radiation. *IEEE Geoscience and Remote Sensing Letters, 10,* 401–405.

Cheng, J., & Ren, H. (2012). Land-surface temperature and thermal-infrared emissivity. In S. Liang, X. Li, & J. Wang (Eds.),

Advanced remote sensing: terrestrial information extraction and applications (pp. 235–271). Cambridge: Academic Press.

Cristobal, J., Jimenez-Munoz, J. C., Sobrino, J. A., Ninyerola, M., & Pons, X. (2009). Improvements in land surface temperature retrieval from the landsat series thermal band using water vapor and air temperature. *Journal of Geophysical Research*. doi:10.1029/2008JD010616.

Dong, L. X., Hu, J. Y., Tang, S. H., & Min, M. (2013). Field validation of GLASS land surface broadband emissivity database using pseudo-invariant sand dunes sites in Northern China. *International Journal of Digital Earth, 6,* 96–112.

Garcia-Santos, V., Valor, E., Caselles, V., & Dona, C. (2016). Validation and comparison of two models based on the Mie theory to predict 8–14 um emissivity spectra of mineral surfaces. *Journal of Geophysical Research: Solid Earth, 121,* 1739.

Gillespie, A. (2014). Land surface emissivity. In E. G. Njoku (Ed.), *Encyclopedia of Remote Sensing* (pp. 303–311). New York: Springer.

Gillespie, A. R., Rokugawa, S., Matsunaga, T., Cothern, J. S., Hook, S. J., & Kahle, A. B. (1998). A temperature and emissivity separation algorithm for advanced spaceborne thermal emission and reflection radiometer (ASTER) images. *IEEE Transactions on Geoscience and Remote Sensing, 36,* 1113–1126.

Hapke, B. (2012). *Theory of reflectance and emittance spectroscopy*. Cambridge: Cambridge University Press.

Jimenez-Munoz, J. C., Cristobal, J., Sobrino, J. A., Soria, G., Ninyerola, M., & Pons, X. (2009). Revision of the single-channel algorithm for land surface temperature retrieval from Landsat Thermal-Infrared data. *IEEE Transactions on Geoscience and Remote Sensing, 47,* 339–349.

Li, X., Strahler, A. H., & Friedl, M. A. (1999). A conceptual model for effective directional emissivity from nonisothermal surfaces. *IEEE Transactions on Geoscience and Remote Sensing, 37,* 2508–2517.

Li, Z., Tang, B., Wu, H., Ren, H., Yan, G., Wan, Z., et al. (2013a). Satellite-derived land surface temperature: Current status and prespectives. *Remote Sensing of Environment, 131,* 14–37.

Li, Z.-L., Wu, H., Wang, N., Qiu, S., Sobrino, J.A., Wan, Z.-M., Tang, B.-H., & Yan, G.-J. (2013a). Land surface emissivity retrieval from satellite data. *Internationl Journal of Remote Sensing*, *34,* 3084–3127.

Liang, S. (2001). An optimization algorithm for separating land surface temperature and emissivity from multispectral thermal infrared imagery. *IEEE Transactions on Geoscience and Remote Sensing, 39,* 264–274.

Liang, S., Zhao, X., Liu, S., Yuan, W., Cheng, X., Xiao, Z., et al. (2013). A long-term global land surface satellite (GLASS) data-set for environmental studies. *International Journal of Digital Earth, 6,* 5–33.

Mie, G. (1908). Beitrage zur optik truber medien speziell kolloidaler metrllosungen (Contribution to the optics of turbid media, particulary of colloidal metal solutions). *Annual of Physics, 25,* 377–445.

Mishchenko, M. I., & Macke, A. (1997). Asymmetry parameters of the phase function for isolated and densely packed spherical particles with multiple internal inclusions in the geometric optics limit. *Journal of Quantitative Spectroscopy and Radiative Transfer, 57,* 767–794.

Mishchenko, M. I., Travis, L. D., & Lacis, A. A. (2002). *Scattering, Absorption, and Emission of Light by Small Particle*. Cambridge: Cambridge University Press.

Pitman, K. M., Wolff, M. J., & Clayton, G. C. (2005). Application of modern radiative transfer tools to model laboratory quartz emissivity. *Journal of Geophysical Research*. doi:10.1029/2005JE002428.

Qin, Z., & Karnieli, A. (2001). Mono-window algorithm for retrieving land surface temperature from Landsat TM data and its application to the Israel–Egype border region. *International Journal of Remote Sensing, 22,* 3719–3746.

Sobrino, J. A., Jiménez-Muñoz, J. C., Sòria, G., Romaguera, M., Guanter, L., Moreno, J., et al. (2008). Land surface emissivity retrieval from different VNIR and TIR sensors. *IEEE Transactions on Geoscience and Remote Sensing, 46,* 316–327.

Spitzer, W. G., & Kleinman, D. A. (1961). Infrared lattice bands of quartz. *Physical Review, 121,* 1324–1335.

Tardy, B., Rivalland, V., Huc, M., Hagolle, O., Marcq, S., & Boulet, G. (2016). A software tool for atmospheric correction and surface temperature estimation of Landsat infrared thermal data. *Remote Sensing, 8,* 696.

Valor, E., & Caselles, V. (1996). Mapping land surface emissivity from NDVI: Application to European, African, and South American areas. *Remote Sensing of Environment, 57,* 167–184.

Wan, Z., & Li, Z.-L. (1997). A Physics-based algorithm for retrieving land-surface emissivity and temperature from EOS/MODIS data. *IEEE Transactions on Geoscience and Remote Sensing, 35,* 980–996.

Xue, Y., Cai, G., Guan, Y. N., Cracknell, A. P., & Tang, J. (2005). Iterative self-consistent approach for earth surface temperature determination. *International Journal of Remote Sensing, 26,* 185–192.

Zhou, J., Li, J., Zhang, L., Hu, D., & Zhan, W. (2012). Intercomparison of methods for estimating land surface temperature from a Landsat-5 TM image in an arid region with low water vapour in the atmosphere. *International Journal of Remote Sensing, 33,* 2582–2602.